Biophysical Journal, Volume *119*

Supplemental Information

Diurnal Variations in the Motility of Populations of Biflagellate Microalgae

Di Jin, Jurij Kotar, Emma Silvester, Kyriacos C. Leptos, and Ottavio A. Croze

Diurnal variations in the motility of populations of biflagellate microalgae: supporting material

D. Jin[1*], J. Kotar[1], E. Silvester[3], K. C. Leptos[2], O. A. Croze[1*]

[1]Cavendish laboratory, University of Cambridge, Cambridge CB3 0HE, United Kingdom

[2]Department of Applied Mathematics and Theoretical Physics, University of Cambridge, Cambridge CB3 0WA, United Kingdom

[3]Clarendon Laboratory, University of Oxford, Oxford OX1 3PU, United Kingdom

[*]oac24@cam.ac.uk, di.jin@weizmann.ac.il

Supplementary figures

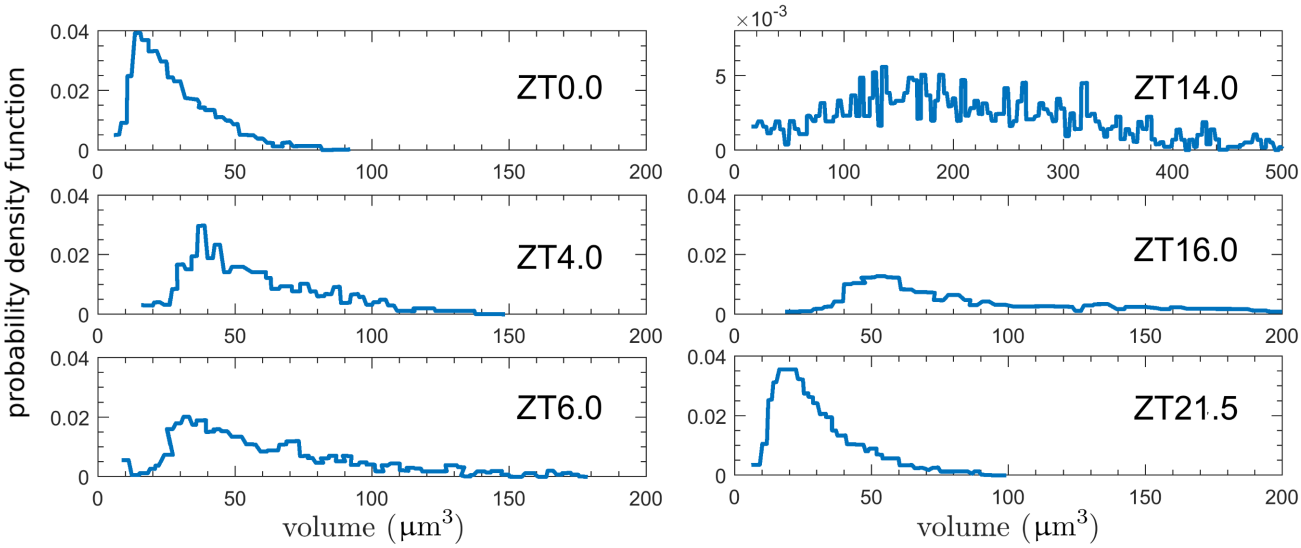

Figure S1 Cell volume distributions at different Zeitgeber times obtained from Coulter counter measurements.

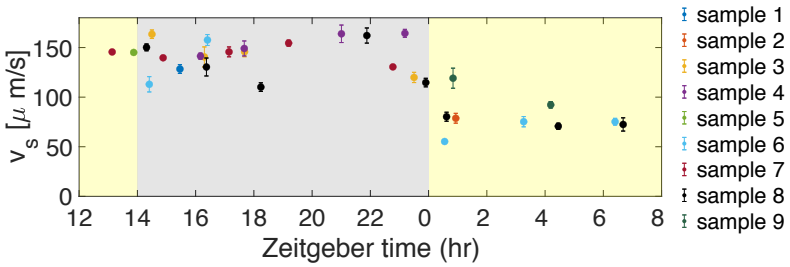

Figure S2 Swimming speeds measured for the nine independent cultures.

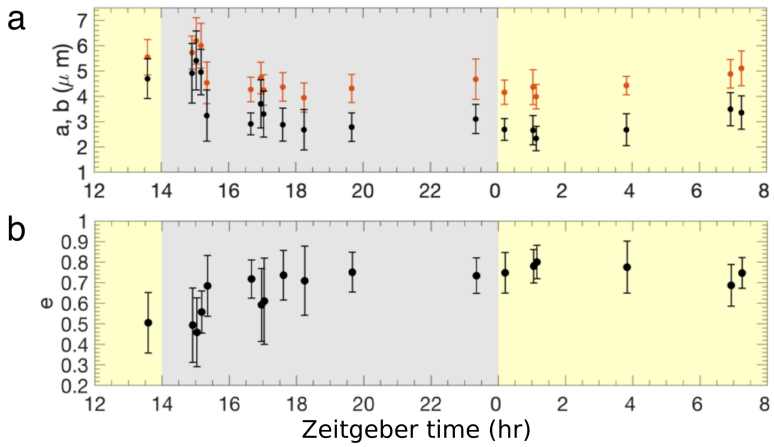

Figure S3 a) Average major axis a (orange) and average minor axis b (black). b) Cell eccentricity, defined as $e = \sqrt{1 - b^2/a^2}$, $e = 0$ represents a spherical shape.

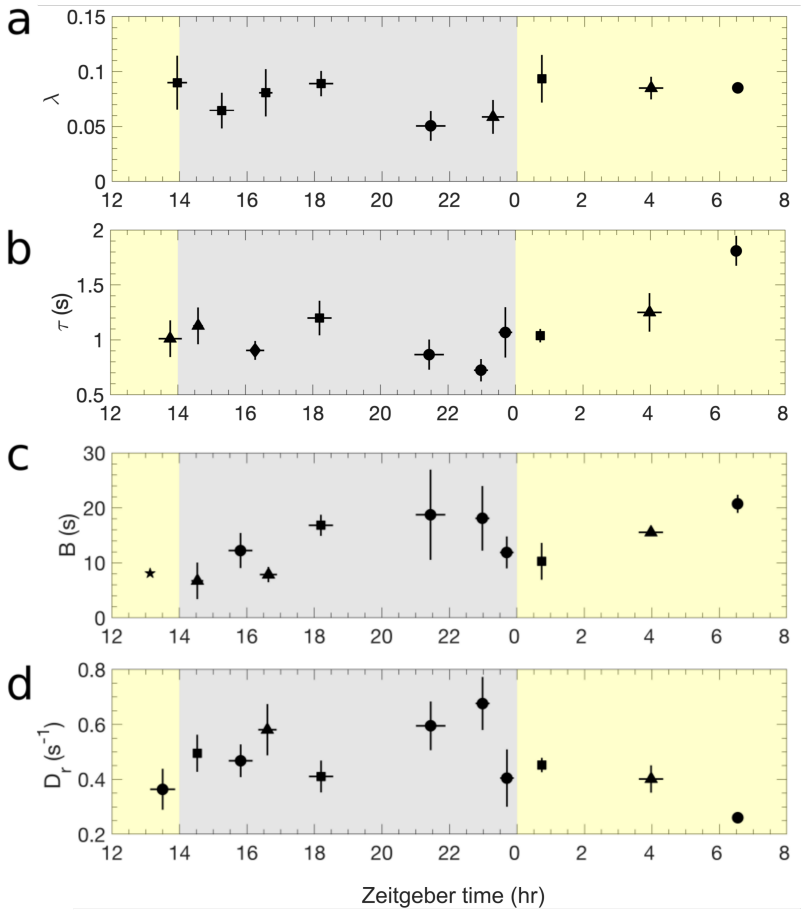

Figure S4 a) Bias parameter. b) Decorrelation time. c) Gravitactic parameter. d) Rotational diffusivity. Symbols ★, ●, ▲, and ■ represent sample sizes of 1, 2, 3 and 4 respectively.

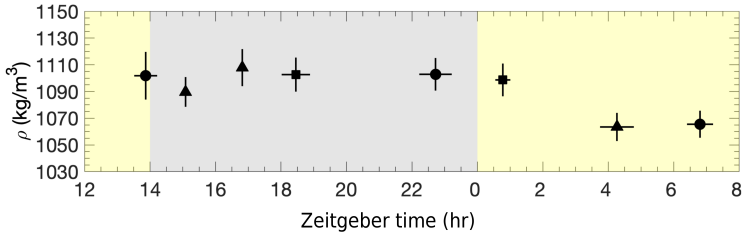

Figure S5 Mass density of cells. Symbols ●, ▲, and ■ represent sample sizes of 2, 3 and 4 respectively.

Supplementary methods

Individual-based simulation of gravitactic cell trajectories for evaluating D_r and B

We carried out individual-based simulations to derive the relations between relevant parameters and rotational diffusivity as a tool to estimate rotational diffusivity from the collected 2D projected trajectories. In the simulations, cells are represented as point objects, which implies that the volumes of the cell bodies do not affect the hydrodynamics, and cell-cell interaction can be ignored. This is justified by the following. The flow velocity around a swimming cell decays away from the cell boundary to 1% of the swimming speed in 7 cell radii[1]. In our experiments, the maximum cell number density is 2.6×10^6 cells/ml, corresponding to a mean cell spacing of 0.07 mm, in which limit cell-cell interaction is negligible[2]. Cells are assumed to be spherical, and the viscosity of the suspension is assumed to be approximately equal to the viscosity of water, which is justified

by the low volume fraction of cells ($\sim 10^{-3}$)[3]. The governing equations are described as in[4]

$$\frac{\mathrm{d}\mathbf{p}}{\mathrm{d}t} = \frac{1}{2B}[\mathbf{k} - (\mathbf{p}\cdot\mathbf{k})\mathbf{p}] + \Gamma_{\mathbf{r}} \tag{1a}$$

$$\frac{\mathrm{d}\mathbf{x}}{\mathrm{d}t} = v_{\mathrm{s}}\mathbf{p} \tag{1b}$$

where $\mathbf{p}$ is the cell swimming orientation, $\mathbf{k}$ is a unit vector pointing upwards (antiparallel to the acceleration of gravity), B is the gravitactic reorientation time and v_s is the swimming speed, as in the main text. The noise Γ_r is added to simulate the stochastic rotational diffusivity of a swimming cell. In the absence of gravitactic reorientation, the cell orientation $\mathbf{p}$ undergoes rotational diffusion and the trajectory of $\mathbf{p}$ is a random walk on a sphere. This process can be numerically simulated by generating a random unit vector $\mathbf{p}'$ and superposing it onto the original $\mathbf{p}$, a method adopted from Thorn & Bearon[5]. $\mathbf{p}'$ is generated via the polar angles $\theta' \sim \mathrm{N}(0, 4D_{\mathrm{r}}\delta t)$ and $\phi' \sim \mathrm{U}[0, 2\pi]$, where δt is the time step[5,6]. The set of ODEs was discretised explicitly using the Euler forward method as the following

Predictor step:

$$\mathbf{p}^* = \mathbf{p}_{\mathrm{n}} + \delta t \frac{1}{2B}[\mathbf{k} - (\mathbf{p}_{\mathrm{n}}\cdot\mathbf{k})\mathbf{p}_{\mathrm{n}}] + \sqrt{2D_{\mathrm{r}}}\delta\mathbf{W} \tag{2a}$$

$$\mathbf{x}^* = \mathbf{x}_{\mathrm{n}} + \delta t\ v_{\mathrm{s}}\mathbf{p}_{\mathrm{n}} \tag{2b}$$

Corrector step:

$$\mathbf{p}_{\mathrm{n+1}} = \mathbf{p}_{\mathrm{n}} + \frac{1}{2}\delta t \left\{ \frac{1}{2B}[\mathbf{k} - (\mathbf{p}_{\mathrm{n}}\cdot\mathbf{k})\mathbf{p}_{\mathrm{n}}] + \frac{1}{2B}[\mathbf{k} - (\mathbf{p}^*\cdot\mathbf{k})\mathbf{p}^*] \right\} + \sqrt{2D_{\mathrm{r}}}\delta\mathbf{W} \tag{3a}$$

$$\mathbf{x}_{\mathrm{n+1}} = \mathbf{x}_{\mathrm{n}} + \frac{1}{2}\delta t\ (v_{\mathrm{s}}\mathbf{p}_{\mathrm{n}} + v_{\mathrm{s}}\mathbf{p}^*) \tag{3b}$$

where $\sqrt{2D_{\mathrm{r}}}\delta\mathbf{W}$ represents the stochastic rotational diffusion step[5].

To investigate the effects of the initial condition on the decorrelation rate of $\mathbf{p}$, from which D_{r} is estimated, the initial $\mathbf{p}$ values were generated from a uniform distribution in the $\mathbf{p}$ space on a unit sphere

$$\theta_0 = \mathrm{acos}(2b - 1) \quad \text{where } b \sim \mathrm{U}[0, 1]$$

or from the steady-state von Mises distribution[7], which corresponds to the experiment

$$f(\cos\theta) = \frac{\lambda e^{\lambda\cos\theta}}{2\sinh\lambda}, \quad \text{where} \quad \lambda = (2BD_{\mathrm{r}})^{-1} \tag{4}$$

In both cases, $\phi_0 \sim \mathrm{U}[0, 2\pi]$. The ODE system was solved with a Fortran program parallelised with OpenMP.

More than 500 cell trajectories were simulated, and the decorrelation time τ, defined to be the characteristic time of the exponential decay of the autocorrelation function, $\langle\cos(\theta(t_0))\cdot\cos(\theta(t_0+\delta t)\rangle$, was evaluated as a function of D_{r} for different values of the bias parameter $\lambda = 1/(2BD_{\mathrm{r}})$ in the range of $0.1 - 2.2$ (Figure S6 a). The relation can be well represented by $\tau = A/D_{\mathrm{r}}$ statistically, and $A(\lambda)$ was obtained by a linear fit, (Figure S6 b). The analysis was performed with directional autocorrelation functions of both θ and its projection in the x-z plane, θ_{p}.

Both the initial distribution of the cell orientations and projection bias significantly affect the relation between D_{r} and τ, as evident in Figure S7. Using the fitted relation of $A = 0.026\lambda^3 - 0.093\lambda^2 - 0.05\lambda + 0.48$ for steady-state initial cell orientation distribution and projected angles, D_{r} is evaluated from experimental trajectories. It follows, as described in the main text (see Materials and Methods), that B is evaluated from the definition of $\lambda = 1/(2BD_r)$.

Assessing cell mass density

As one of the steps carried out during motility measurements (see Materials and Methods), the capillary was placed in an UV oven ($\times 100$ $\mu\mathrm{J/cm}^2$,®UVP CX-2000 UV Cross Linker) for 5 minutes, which fixed cells without lysing them. The capillary was immediately loaded to the vertical-stage microscope. Five videos were acquired at 5 frames per second for 20 seconds.

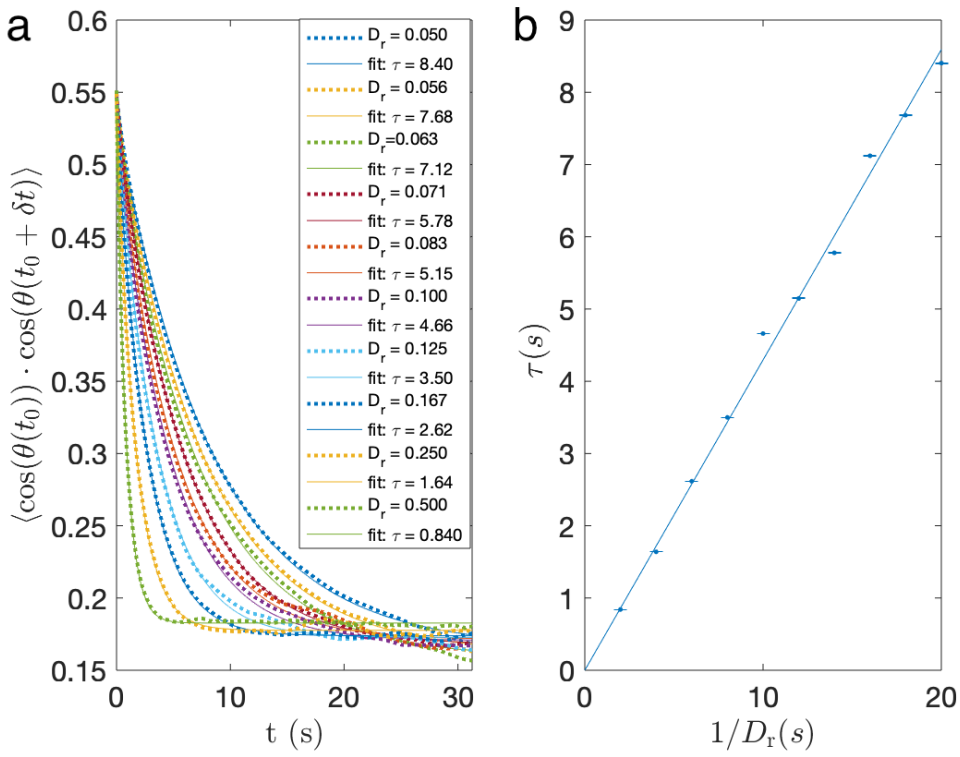

Figure S6 Evaluation of $A(\lambda)$ at λ = 0.6 with an initial steady-state orientation distribution and for projected angles. a) Each auto-correlation function $\langle\cos(\theta(t_0))\cdot\cos(\theta(t_0+\delta t)\rangle$ was obtained with more than 500 trajectories. τ is acquired by fitting an exponential decay function. b) $A(\lambda) = 0.430$ was evaluated as the slope of the linear fit to τ ($1/D_r$). Error bars represent the 95% confidence interval of the exponential decay fit.

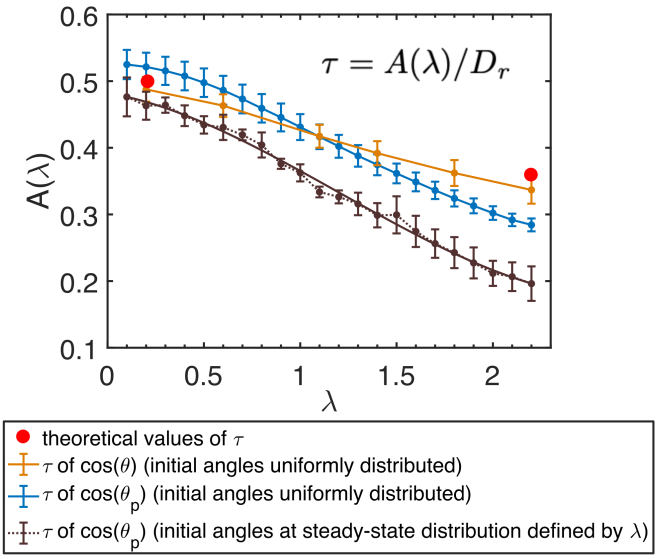

Figure S7 $A(\lambda)$ functions acquired from simulated cell trajectories. The two initial cell orientation distributions are uniform over the unit sphere and the steady-state distribution described in Equation 4. Directional decorrelation time τ was evaluated from simulated trajectories both from the 3D swimming angle θ and its projection in the x-z plane θ_p. The brown solid curve is a fitted polynomial $A = 0.026\lambda^3 - 0.093\lambda^2 - 0.05\lambda + 0.48$, which was applied in the analysis of the experimental data. The simulation yields agreement with two theoretical values by Bearon, Bees, & Croze (2012).

Cell mass densities were calculated from the sedimentation speed of the UV-fixed cells. By assuming that the *Chlamydomonas* cells are spherical, the density of a cell can be evaluated using Stokes' law

$$\rho_{\text{cell}} = \frac{9}{2}\frac{\mu v_{\text{set}}}{gR^2} + \rho_{\text{water}}, \tag{5}$$

where the average settling velocity v_{set} and cell radius R were evaluated for individual trajectories. R was determined by a function within the MATLAB IDL algorithm[8], which identifies the centres of the cells as the local maximas in the grey-scale image and evaluates the squared radius of gyration of the surrounding pixel intensities. The cell radius statistics were cross-checked with Coulter counter measurements. The average number of cell trajectories in each recording is 1240.

Supplementary results

Reorientation dynamics of Chlamydomonas gravitaxis

Parameter λ indicates the up-swimming bias of the cell population, and for *C. reinhardtii*, $\lambda \approx 0.051 - 0.094$ (figure S4 a). This value is much lower than the commonly quoted $\lambda = 2.2$ measured with *C. augustae*[29]. Qualitatively, the cell trajectories do not manifest a clear collective upward trend as presented in Hill & Hader (1997) with *C. augustae*. The directional decorrelation time τ increases during the light period, indicating longer persistent "runs" (figure S4 b). In the post-mitotic dark period ZT18-23, as the daughter cells hatch and replace the mother cells in the cell population, B increases in comparison to ZT14-18 (figure S4 c). An explanation could be the consumption of starch[11]. Starch has a higher density of $1.29 - 1.34$ g/cm^3 than the average cell density, and it accumulates around the pyrenoid at the rear end of the cell[12]. Bottom-heaviness can be reduced due to its consumption, which leads to a smaller offset between the geometric centre and the centre of mass. The average value of B is 13.8 s, which is greater than 5.1 ± 0.7 s measured with immoblised CC-125 wt cells by Yoshimura and coworkers[13]. Yoshimura and coworkers also examined the reorientation dynamics of immoblised mutants *gtx*1 and *gtx*2, which were demonstrated to be gravitaxis-deficient when actively swimming. It concluded that the up-swimming bias attributes not only to the passive bottom-heaviness property but also to an active gravisensing mechanism since no significant variation was found between the immobilised wild type cells and immobilised gravitaxis-deficient cells. The greater value of B of active wild type CC-125 cells reported in the current study contradicts with the hypothesis since a stronger gravitactic effect is not seen when comparing with the immobilised wild type cells. It suggests that bottom-heaviness plays a dominant role in gravitactic reorientation, which seems to be destablised when the flagella are engaged in motion. However, there are a few

inconsistencies between the two studies which suggest that further experiments are required to verify the hypothesis. First, because the CC-125 cells in Yoshimura, Matsuo, & Kamiya (2003) were cultured in TAP medium, cells undergo an additional process of acetate assimilation which facilitates gluconeogenesis[14]. Higher starch content may enhance bottom-heaviness by bringing the geometric centre further away from the centre of mass, causing a lower B value. Second, viscous resistance exerted on beating and non-beating flagella can be different, and its relevance is not examined in the comparison between active and immoblised cells. Finally, the data of cell reorientation dynamics in Yoshimura, Matsuo, & Kamiya (2003), were obtained from 5 to 10 independent cell trajectories and at 2 s intervals, which is a smaller data set comparing to the current study.

Rotational diffusivity D_r fluctuates through time in the range of $0.2 - 0.7$ s^{-1}, which is in the same order of magnitude with previously reported measurements for *C. reinhardtii*, $0.05 - 0.3$ s^{-1}[15] and 0.15 s^{-1}[16] (Figure S4 d). Although not as significant as with the case of swimming speed, a lower light period value is also observed with D_r . The origin of rotational diffusion is the occurrence of asymmetric flagellar beating which leads to a net torque on the cell. However, it is known that flagellar motion has rich dynamics: it switches between synchronous and various asynchronous modes, each associated with a distinct beating pattern. This affects cell trajectories, causing helical motion, straight-runs, jittering, and sharp turns[17]. Mapping of flagellar locomotion to trajectory characteristics has yet to be achieved. However, it is reasonable to hypothesise that flagellar beat frequency correlates with the rate of turning events and therefore rotational diffusivity. Indeed, by plotting D_r against the corresponding f at each time point, a trend of positive correlation is observed (Figure S8). Additional experiments of high frequency and high resolution video microscopy will provide evidence of links between flagellar beating and reorientation dynamics to substantiate the hypothesis.

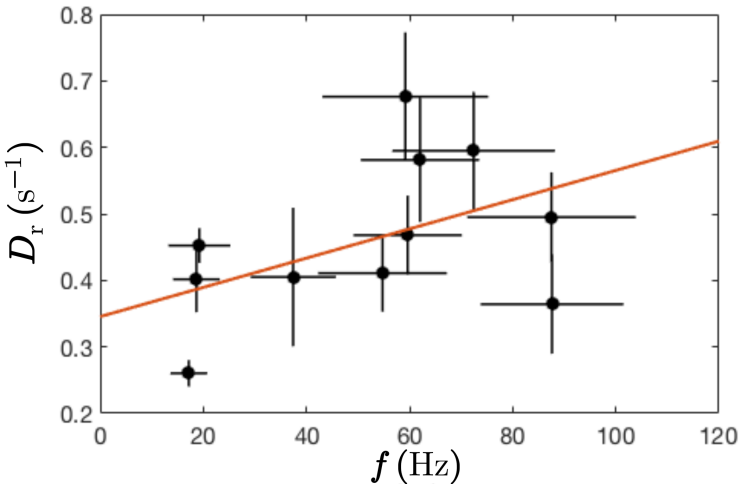

Figure S8 D_r versus beat frequency f at each time point. A linear fit suggests a potential positive correlation.

References

1. Drescher, K., Goldstein, R. E., Michel, N., Polin, M. & Tuval, I. Direct measurement of the flow field around swimming microorganisms. *Phys. Rev. Lett.* **105**, 1–4 (2010).
2. Pedley, T. J. & Kessler, J. O. A new continuum model for suspensions of gyrotactic micro-organisms. *J. fluid mechanics* **212**, 155–182 (1990).
3. Mussler, M., Rafaï, S., Peyla, P. & Wagner, C. Effective viscosity of non-gravitactic *Chlamydomonas reinhardtii* microswimmer suspensions. *EPL (Europhysics Lett.* **101**, 54004 (2013).
4. Croze, O. a., Sardina, G., Ahmed, M., Bees, M. a. & Brandt, L. Dispersion of swimming algae in laminar and turbulent channel flows: consequences for photobioreactors. *J. Royal Soc. Interface* **10**, 20121041 (2013).
5. Thorn, G. J. & Bearon, R. N. Transport of spherical gyrotactic organisms in general three-dimensional flow fields. *Phys. Fluids* **22**, 041902, DOI: 10.1063/1.3381168 (2010).
6. Saragosti, J., Silberzan, P. & Buguin, A. Modeling *E. coli* tumbles by rotational diffusion. Implications for chemotaxis. *PloS one* **7**, e35412 (2012).

7. Pedley, T. J., Kessler, J. O. Hydrodynamic phenomena in suspensions of swimming microorganisms. *Annu. Rev. Fluid Mech.* **24**, 313–358 (1992).

8. Crocker, J. C. & Grier, D. G. Methods of digital video microscopy for colloidal studies. *J. Colloid Interface Sci.* **179**, 298–310 (1996).

9. Vladimirov, V. a., Wu, M. S. C., Pedley, T. J., Denissenko, P. V. & Zakhidova, S. G. Measurement of cell velocity distributions in populations of motile algae. *The J. Exp. Biol.* **207**, 1203–1216 (2004).

10. Hill, N. A. & Hader, D. P. A biased random walk model for the trajectories of swimming micro-organisms. *J. theoretical biology* **186**, 503–526 (1997).

11. Garz, A. *et al.* Cell-to-cell diversity in a synchronized *Chlamydomonas* culture as revealed by single-cell analyses. *Biophysj* **103**, 1078–1086 (2012).

12. Diaz, A. *et al.* Three-dimensional mass density mapping of cellular ultrastructure by ptychographic X-ray nanotomography. *J. Struct. Biol.* **192**, 461–469 (2015).

13. Yoshimura, K., Matsuo, Y. & Kamiya, R. Gravitaxis in *Chlamydomonas* reinhardtii studied with novel mutants. *Plant Cell Physiol.* **44**, 1112–1118 (2003).

14. Johnson, X. & Alric, J. Central carbon metabolism and electron transport in *Chlamydomonas* reinhardtii: Metabolic constraints for carbon partitioning between oil and starch. *Eukaryot. Cell* **12**, 776–793 (2013).

15. Roberts, A. M. Mechanisms of gravitaxis in *Chlamydomonas*. *Biol. Bull.* **210**, 78–80 (2006).

16. Barry, M. *Mechanisms of Reorientation in Phytoplankton: Fluid Shear, Surface Interactions, and Gravitaxis*. Ph.D. thesis, Massachusetts Institute of Technology (2014).

17. Polin, M., Tuval, I., Drescher, K., Gollub, J. P. & Goldstein, R. E. *Chlamydomonas* swims with two "gears" in a eukaryotic version of run-and-tumble locomotion. *Science* **325**, 487 (2009).